Ocean Engineering 197 (2020) 106895

Contents lists available at ScienceDirect

Ocean Engineering

journal homepage: www.elsevier.com/locate/oceaneng

CFD study of ship stopping maneuver by overset grid technique

Jianhua Wang, Decheng Wan *

School of Naval Architecture, Ocean and Civil Engineering, State Key Laboratory of Ocean Engineering, Shanghai Jiao Tong University, Collaborative Innovation Center for Advanced Ship and Deep-Sea Exploration, Shanghai, 200240, China

ARTICLE INFO

Keywords:
Ship stopping maneuver
Overset grid method
Reversing propeller
CFD simulation

ABSTRACT

The crowded waterways and worse maneuverability of large ships could cause more collision accidents. Therefore, it is necessary to study stopping ability of ships to ensure the navigational safety. In this paper, the CFD solver naoe-FOAM-SJTU associated with dynamic overset grid method is used to simulate several types of maneuvers of KVLCC1 ship model. Stopping maneuvers with reversing propeller, turning rudder with/without propeller are simulated to predict the ship stopping performance. Turning circle maneuver is also simulated to predict the advance and comparisons with stopping distance of other stopping maneuvers are discussed. Self-propulsion simulation is conducted firstly to validate the present CFD approach through comparisons with available experiments. Stopping maneuver simulations start from the steady state of self-propulsion, then different types of stopping maneuver is carried out by controlling the propeller and rudder. In addition, deep and shallow water conditions are both computed to illustrate the water depth effect on the stopping performance. The predicted trajectory and ship speed of different stopping maneuvers are presented and analyzed. Detail information of flow visualizations including pressure distribution and wake flow during stopping maneuver are discussed to explain the stopping behavior. It is concluded that the turning circle maneuver is the most preferable way to avoid the collision in open sea. However, if the ship needs to stop in port or waterways, then the reversing propeller (RP) is better due to the fact that it meets the relatively shorter lateral deviation.

1. Introduction

In recent years, cargo ships such as container ship, bulk carrier, tend to become larger to reduce the cost of shipping and thus improve transport efficiency. However, a larger size of ship will worsen the maneuverability, and accidents can easily occur in the crowded ports or channels. Therefore, it is of great importance to study the stopping ability of large ships to prevent the ship from collision and to ensure the safety of a ship sailing near the port, especially in shallow water.

Since the operation on propeller and rudder changes the course of ship, the trajectory of stopping maneuver is not a straight line, as shown in Fig. 1. Good stopping ability means minimum stopping distance (also known as track reach), horizontal distance (or lateral distance) and yaw angle. Generally, reversing propeller is the most common operation when a large ship needs to brake to prevent collision. In the procedure of stopping maneuver, the bow will turn port or starboard side because of the side forces at the aft caused by the reversing propeller. The existence of the lateral force caused by reversing propeller is found by Chislett and Smitt (1972) through ship model test. Apart from the reversing propeller approach, several other operations on propeller and rudder, such as turning rudder while reversing propeller, turning rudder while stopping the engine, also have some influences on the stopping ability. When the obstacle is in the open sea, turning circle maneuver can also be a preferable way to avoid the collision while in the meantime reduce the load of engine.

The stopping ability is a key standard to examine the ship performance. Traditionally, empirical formula method and experimental method are used to evaluate the stopping ability of ships. The requirements of an actual ship stopping experiment with free running facility are very difficult to achieve and the test cost is very high. Therefore, estimation of ship stopping ability through numerical simulation is preferred. At present, numerical study of ship stopping maneuver still relies on captive model test. At first, mathematical model is established and the related hydrodynamic derivatives are separated. Then the ship hydrodynamic is predicted through either experiments or numerical simulations. At last, the ship maneuvering motion is calculated from the obtained parameters. Two kinds of mathematical model, i.e. Abkowitz model (Abkowitz, 1980) and MMG model (Yasukawa and

* Corresponding author.
E-mail address: dcwan@sjtu.edu.cn (D. Wan).

https://doi.org/10.1016/j.oceaneng.2019.106895
Received 16 May 2019; Received in revised form 6 December 2019; Accepted 23 December 2019

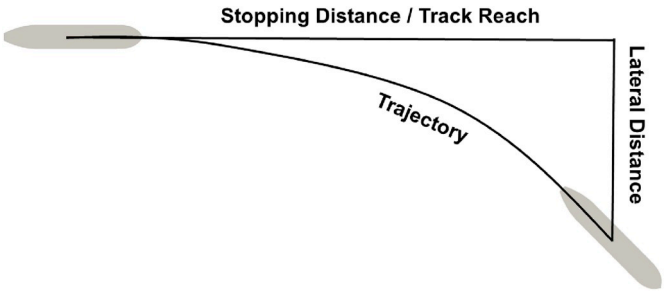

Fig. 1. Stopping trajectory of the ship using reversing propeller.

Yoshimura, 2015), were proposed to describe the maneuvering motion equations with different aspects of the way of the forces acting on the ship, propeller and rudder and their interaction. This approach has been widely used in the prediction of ship stopping ability.

Crane (1967) used a non-linear mathematical model with experimentally determined coefficients approach to do computations of stopping maneuvers. It was concluded that the merits of various methods for improving stopping performance depend largely on ship speed-of-approach. Hooft (1970) presented the results of model experiments on a "Series-60" model regarding the governing factors in respect of the controllability during the stopping maneuver and gave a quasi-stationary solution of the equations of motion in the horizontal plane. Dong et al. (1996) used a mathematical model to compute ship motion in crash stopping and proposed a new method to deal with hydrodynamic forces and moments of propeller based on the principle of ship propulsion and maneuverability. Good agreements were achieved by comparing with sea trials and experiments. Lu (2007) conducted simulations of ship stopping motion by reverse propulsion, where the stopping maneuver was calculated based on MMG model. Yabuki et al. (2006) conducted experimental and numerical studies that aimed at investigating the characteristics of the stopping motion of a ship with a single controllable pitch propeller (CPP) and single rudder. They used the mathematical model and considered the wind force. Ueno et al. (2017) carried out numerical predictions for stopping maneuver of model scale KVLCC1 ship and proposed a J and speed correction (JSC) method to give predictions of full scale ship performance. The stopping maneuver is simulated based on a three-degree-of-freedom mathematical model. Free running model tests on ship stopping maneuver were also performed and compared with the numerical results.

Although the most previous researches of stopping maneuver using mathematical model are convenient, they cannot analyze the detailed interaction between the propeller and the ship. Among several approaches to predict ship maneuverability, numerical simulation of free running ship with actual rotating propellers and turning rudders is the most reliant way to predict the complex flow interactions during ship maneuvering motion. So far, dynamic overset grid technique has been successfully applied to solve the problem of large amplitude ship motions and complex motion of ship hull-propeller-rudder interaction. Carrica et al. (2012) performed the simulations of turn and zigzag maneuver using a self-developed solver CFDShip-Iowa and the operation of rudders were achieved by the dynamic overset grid technique, while the rotating propellers were using body force model. Mofidi and Carrica (2014) further extended their work by using the direct simulation of free-running zigzag maneuver of KCS ship model, where ship maneuver with actual rotating propeller and turning rudder were computed in calm water. The results were promising when compared with the experiment, although the authors emphasized that the computational cost in direct calculating free-running ships was still very high. After that, Carrica et al. (2016) further investigated the direct simulation of zigzag maneuver of KCS ship model in shallow water. Recently, Dubbioso et al. (2017) and Muscari et al. (2017) conducted CFD investigations of hydrodynamic loads on propellers in steady and transient maneuvers using overset grid approach. Shen et al. (2015) implemented the dynamic overset grid module to the open source CFD software OpenFOAM and presented some applications to the ship maneuvering motions. Wang et al. (2017, 2018) used the same approach to simulate the free running ship with applications to self-propulsion, zigzag maneuver, turning circle maneuver in both calm water and waves, which showed that the dynamic overset grid approach is a suitable and reliable way to predict strong interactions between ship hull, propeller and rudder.

In the present paper, the author uses the self-developed naoe-FOAM-SJTU solver (Wang et al., 2019a) based on overset grid technique to directly simulate the ship stopping maneuver with rotating propellers and turning rudders. The main purpose of this study is to propose an accurate way to predict the performance of ship stopping maneuver based on viscous flow computations. Actually, this study not only considers the standard stopping maneuver (also known as the full astern stopping maneuver), but also carries out other types of maneuvers with the purpose of investigating the different ship performance through the operation on propeller and rudder. Main parameters of stopping maneuver, such as the stopping distance, the lateral distance, are presented and compared with the available experiment. Detailed analysis and

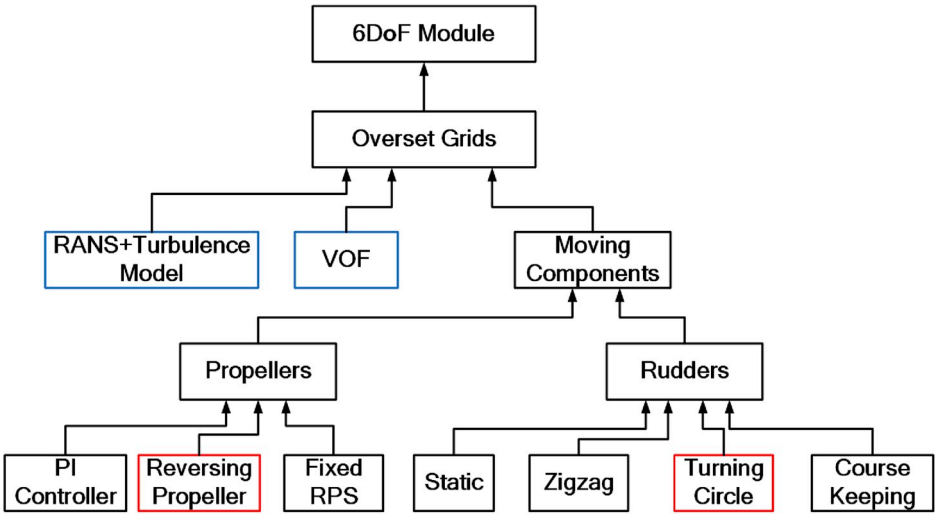

Fig. 2. Diagram of 6DoF motion with moving components.

Fig. 3. Geometry model of KVLCC1.

comparison of the pressure distribution and the wake flow around the ship are also presented.

The paper is organized as follows. Numerical methods including the naoe-FOAM-SJTU solver and numerical schemes are illustrated. Then the geometry model, computational grid, are presented. Self-propulsion simulation is discussed firstly and then the detailed simulations of different types of maneuvers, i.e. reversing propeller, no propeller case (inertia stop case), turning circle are described subsequently. Finally, a brief conclusion is drawn.

2. Numerical methods

In the present study, numerical simulations for ship stopping maneuvers are performed with the ship hydrodynamics CFD solver, naoe-FOAM-SJTU, which is developed on the open source platform OpenFOAM and has the overset grid capability. The solver includes a full 6DoF motion module with a hierarchy of bodies. Therefore, it is very convenient to achieve the numerical computations of free running ship. Based on the dynamic overset grid module and the 6DoF motion with moving component, different kinds of ship maneuvers can be simulated. So far, the present solver has the ability of simulating ship self-propulsion, zigzag maneuver, turning circle maneuver and course keeping maneuver based on the control of movement of propeller and rudder.

Fig. 2 illustrates the diagram of the 6DoF motion module in naoe-FOAM-SJTU solver. The original modules in OpenFOAM, such as RANS, VOF and turbulence models, are marked with blue color. These modules are further modified for sparse matrix solvers to excluded non-active cells when using dynamic overset grid. The stopping maneuver in the present study is simulated incorporating with the reversing propeller (marked in red color) module. As we know, it is rather difficult to reappear the actual operations in test case using CFD computations. Furthermore, the present work mainly focuses on the integral values of stopping maneuver, such as trajectory and velocity, which are more or less dominated by the effects after the full astern execution. Considering the above aspects, here we adopt the constant deacceleration approach to achieve the reversing control of the propeller. The control mechanism of reversing propeller is by deaccelerate the rotational speed of propeller through

$$R_{RP} = \begin{cases} R_0 - kt & t \le t_p \\ -R_0 & t > t_p \end{cases} \quad (1)$$

where R_{RP} is the rotational speed of reversing propeller, R_0 is the original speed according to the corresponding ship speed, k is the propeller accelerating rate (here we use constant value 5.18r/s^2) and t_p is the time when the rotational speed achieves the target value. In addition, turning circle maneuver is also used when considering the rudder reflection.

Table 1
Main particulars of KVLCC1 ship model.

Main particulars	Symbols	Model scale (1:110)
Length of waterline	$L_{pp}(m)$	2.9091
Maximum beam of waterline	$B_{WL}(m)$	0.5273
Draft	$T\ (m)$	0.1891
Displacement	$\Delta(m^3)$	0.2349
Longitudinal coordinate of center of gravity	$x_G(m)$	0.1009
Metacentric height	$GM\ (m)$	0.1099
Wetted surface area (without rudder)	$S_0(m^2)$	2.2475
Radii of inertia	K_{xx}/B	0.40
	K_{yy}/L_{WL}, K_{zz}/L_{WL}	0.25
Propeller diameter	$D_P(m)$	0.09
Propeller rotation direction		Right-hand
Rudder type		Horn
Maximum rudder rate	$(\text{deg.}/s)$	24.5

For the flow field calculation, the present naoe-FOAM-SJTU solves the Reynolds-averaged Navier-Stokes (RANS) equations for unsteady turbulent flows around the advancing ship. A volume of fluid (VOF) approach with bounded compression technique is used (Berberović et al., 2009) to capture the free surface. The turbulence features are modeled by a blended $k-\omega/k-\varepsilon$ shear stress transport (SST) turbulence model (Menter et al., 2003). The velocity gradient near the wall is resolved by the wall function treatment. Up to now, the naoe-FOAM-SJTU solver has been extensively validated various ship hydrodynamic cases, e.g. ship resistance (Zha et al., 2014, 2015), sea-keeping (Shen and Wan, 2013, 2016; Shen et al., 2014), propulsion and maneuvering (Shen et al., 2015; Wang et al., 2017, 2018; 2019b; Wang and Wan, 2018).

The finite volume method (FVM) with unstructured grids is used to transform the governing equations from the physical space into the computational space. The solution of the coupling velocity and pressure equations is obtained by using the pressure implicit with splitting of operator (PISO) algorithm (Issa, 1986). Built-in numerical schemes provided by OpenFOAM are used to discretize the PDEs and supported solvers are employed to solve the linear system of equations.

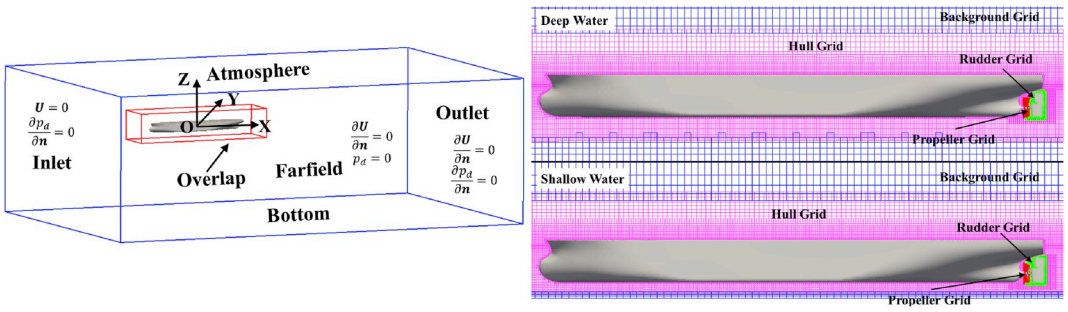

(a) Computational Domain (b) Overset grid distribution

Fig. 4. Computational domain and grid arrangement (a) Computational Domain (b) Overset grid distribution.

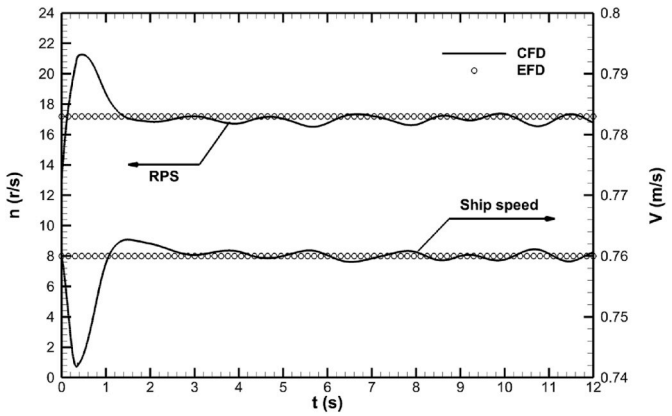

Fig. 5. Time histories of rotational speed of propeller and instantaneous ship speed.

3. Geometry model and grid

3.1. Geometry model

The benchmark ship model KVLCC1 is used for the numerical simulations of ship stopping maneuver. KVLCC1 is a single-screw ship and it has been used as one of the benchmark models for CFD computation in previous 2008 SIMMAN Workshop. The geometric model is shown in Fig. 3 and main particulars of the ship model are listed in Table 1.

3.2. Computational grid and boundary conditions

The computational domain is divided into three parts: the background grid, the grid around the hull and the grid around propeller. The unstructured grids are generated by the tool snappyHexMesh with the background grid generated by blockMesh. As mentioned in the Introduction part, there are several computational grids used in the present work with consideration of different simulation conditions. Fig. 4 shows the computational domain and overset grid arrangement in deep water and shallow water, respectively. In the present simulations, the background domain extends to $-1.5L < x < 3.0L$, $-1.5L < y < 1.5L$, $-1.0L < z < 0.5L$, and the range of hull domain is $-0.15L < x < 1.2L$, $-0.15L < y < 0.15L$, $-0.2L < z < 0.2L$. For the shallow water case, the range of z axis is the same with the corresponding water depth. The grid spacing near wall is designed to meet the requirements using wall functions with y^+ is around 30. The total grid number is 4.58 million and 4.35 million for the deep and shallow water case, respectively.

The boundary conditions are shown in Fig. 4a. The coordinate system and the definition of axis have also been shown in Fig. 4a. The ship is moving forward instead of using inlet velocity. Thus, the upstream boundary condition imposes zero velocity and zero gradient of pressure. Boundary conditions at downstream are identical with pressure outlet condition. For the deep-water case, the bottom boundary condition imposes farfield condition, while non-slip boundary condition is applied for the bottom in shallow water case. The grid size in the upstream and downstream is relatively coarse with the consideration of avoid reflection of ship waves by numerical dissipation.

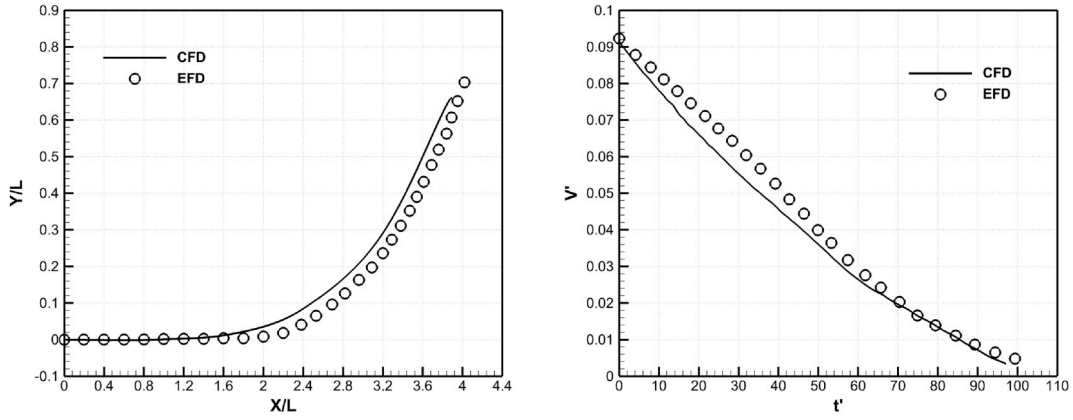

Fig. 6. Comparison of the trajectory and ship speed (a) Trajectory comparison (b) Ship speed comparison.

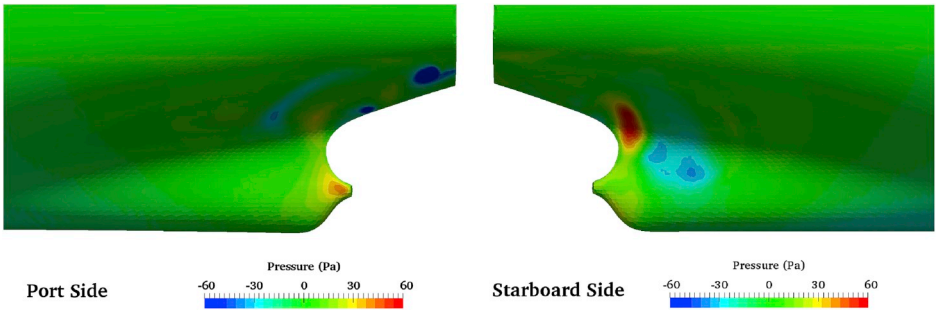

Fig. 7. Pressure distribution on the aft of the ship hull for RP no rudder case ($t' = 18.35$).

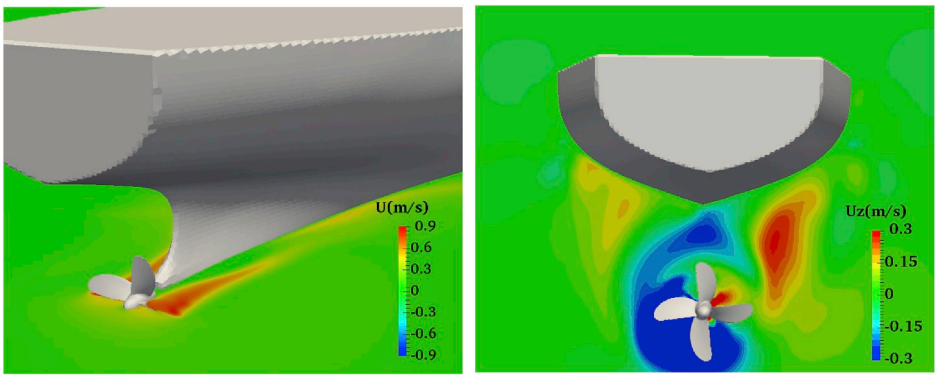

Fig. 8. Wake flow around ship hull and propeller for RP no rudder case (t′ = 18.35) (a) Horizontal section (b) Cross section.

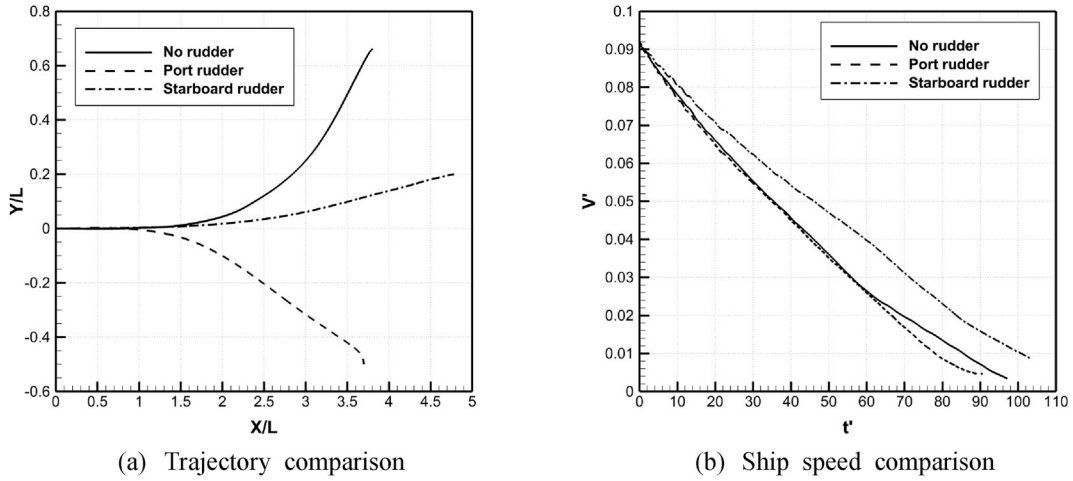

Fig. 9. Trajectory and ship speed comparison of different stopping maneuvers (a) Trajectory comparison (b) Ship speed comparison.

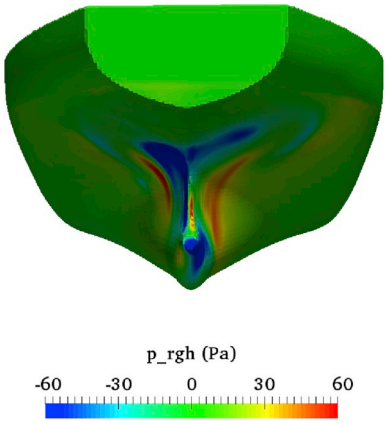

Fig. 10. Pressure distribution on the aft of the ship for RP port rudder case (t′ = 18.35).

4. Numerical simulations and discussions

In the present work, the self-propulsion case is conducted firstly to validate the present CFD solver in predicting the hydrodynamic performance of free running KVLCC1 ship model with rotating propeller. For the stopping maneuver using reversing propeller, three conditions are considered: no rudder, port rudder and starboard rudder. For the no propeller case (inertia stop case), port rudder and starboard rudder are carried out. In the end, a turning circle maneuver is also simulated to estimate the advance. For the turning rudder cases, the turning rate is the maximum rudder rate 24.5 deg./s. All the numerical simulations are conducted on the HPC cluster center in Computational Marine Hydrodynamics Lab (CMHL), Shanghai Jiao Tong University. Each node consists of 2 CPUs with 20 cores per node and 64 GB accessible memory (Intel Xeon E5-2680v2 @2.8 GHz). 40 processors are assigned for each computation. The time step is used to satisfy the requirement of the propeller rotation angle in each time step is no larger than 1°. Thus, the time step is set relatively small with a value of 5×10^{-4} s and the corresponding Courant Number is about 0.15 in all the present simulations.

4.1. Self-propulsion

According to the free running KVLCC1 ship model experiments (Tsukada et al., 2015) performed at National Maritime Research Institute (NMRI) basin, the ship model is advancing in calm water with ship speed of 0.76 m/s (corresponding to the full-scale ship 15.5kn). The ship model is free to trim and sink. During the simulation, the ship speed is an input and a PI controller (Shen et al., 2015) is used to control the rotational speed of propeller to achieve the equivalent between propeller thrust and the ship resistance at the corresponding target ship speed. The self-propulsion simulation starts from the steady state of the towing condition, which means that the initial flow field for the self-propulsion case is mapped from the steady flow of bare hull with

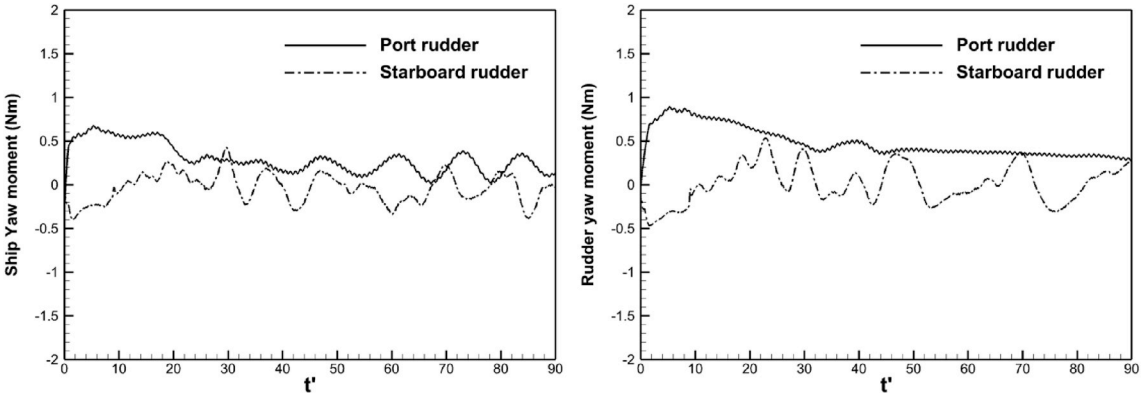

Fig. 11. Comparison of yaw moments between port and starboard rudder cases.

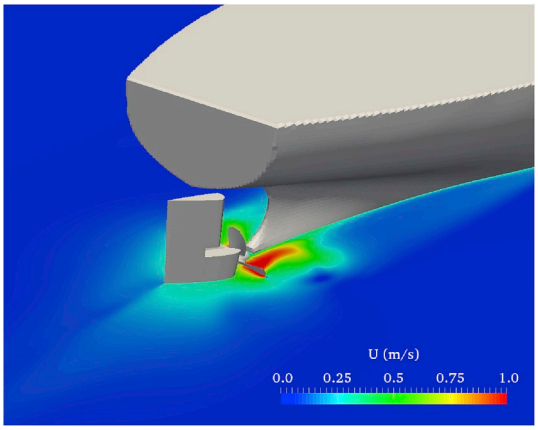

Fig. 12. Wake flow around the propeller and rudder for RP port rudder case (t′ = 18.35).

corresponding ship speed.

Fig. 5 shows the time histories of the calculated rotational speed of propeller and the ship model speed under self-propulsion condition. The predicted results are also compared with the experimental data (Tsukada et al., 2015). It can be seen that the predicted rotational speed of propeller is 17.02 r/s when the ship reaches the target speed. The calculated result is under-predicted by 1.05% compared with the experimental data 17.2 r/s. From the time history of the instantaneous ship speed we can see that the ship speed firstly drops down due to the lower thrust provided by the propeller, and the speed increases as the propeller rate speeds up and finally reaches the target ship speed. It is proved that the numerical approach used in this paper can accurately predict the self-propulsion performance of the KVLCC1 ship model, which lays a good foundation for the simulations of stopping maneuver.

4.2. Reversing propeller

Generally, reversing the propeller is the most common operation when a large ship needs to brake to prevent collision. It is also known as the full astern stopping. The simulation conditions are following the setup of experiments performed at NMRI (Ueno et al., 2017), where the model scale stopping maneuver starts with a speed of 0.4905 m/s (10kn in full scale). Therefore, a self-propulsion simulation at this speed is firstly conducted and the predicted propeller rate of revolution is 10.52 r/s. Since there is no available propeller rate data for this ship speed, thus the full astern propeller rate of revolution (−10.36 r/s) from the experiment (Ueno et al., 2017) is used in the simulation of stopping maneuver. The numerical computation of stopping maneuver starts from the steady state of self-propulsion, then the propeller is controlled to a reverse speed of −10.36 r/s to carry out the crash-astern stopping maneuver. The authors who conducted the stopping maneuver experiments exclude the discussion of the duration time and we cannot do the exactly same control during the simulation. The present simulations adopted the control mechanism as shown in Eqn (1) to deaccelerate the propeller rate. Three degrees of freedom on the horizontal plane, i.e. surge, sway and yaw are released for the numerical simulations of reversing propeller and three conditions are simulated regarding to the rudder, i.e. without rudder, port rudder and starboard rudder. The case of crash-astern case without rudder turning is followed the experimental procedure and has been compared with the available data.

In this case and cases shown later, the non-dimensional parameters are used to identify the ship motion and trajectory. The track reach and lateral distance are expressed as, X/L, Y/L, respectively. Non-dimensional ship speed and time are defined as: $V' = V/\sqrt{gL}$, $t' = t/\sqrt{L/g}$, where L is the ship length and g is the acceleration of gravity. The track reach and the lateral distance is calculated from the beginning point (when the ship executes full astern) to the end point when the ship speed is equals zero. Fig. 6 shows the trajectory and ship speed comparisons between calculated results and the experimental data from NMRI (Ueno et al., 2017). Because the x axis is point to the ship stern and the ship is advancing in the negative axis. In the present paper, the figure is mirrored in x axis. It can be seen from the trajectory that the track reach and the lateral distance agree well with the experimental data. The end point for simulation result is (3.90, 0.673) is very close to the experimental measurement (4.02, 0.703). The CFD result of stopping track is underestimated by 2.98% and the CFD result of lateral distance is 4.27% smaller than the experiment.

The predicted ship speed as shown in Fig. 6b matches well with the experiment for the time to complete stopping maneuver, while some discrepancies are observed for the ship speed during the stopping process. The predicted ship speed is smaller than that of the experimental data during the process, which lead to the shorter travelled distance shown in Fig. 6a. The overall agreement for the present simulation for the stopping maneuver indicates that the CFD approach adopted in this paper can accurately forecast the relevant parameters of stopping maneuver using reversing propeller, providing an alternative way to evaluate ship stopping ability.

An interesting phenomenon can be noticed that the ship turns to the starboard side and the lateral distance can be as large as 0.7L. In order to find out the cause of ship turning, the pressure distribution on the stern and the wake flow around ship hull and propeller are presented and analyzed. The distribution of dynamic pressure on the ship hull at time instant t′ = 18.35 is shown in Fig. 7. It can be seen that a high pressure zone on the starboard side of the aft hull is appeared during the stopping maneuver, while the change of pressure distribution on the port side is very small compared with the starboard side. The different pressure

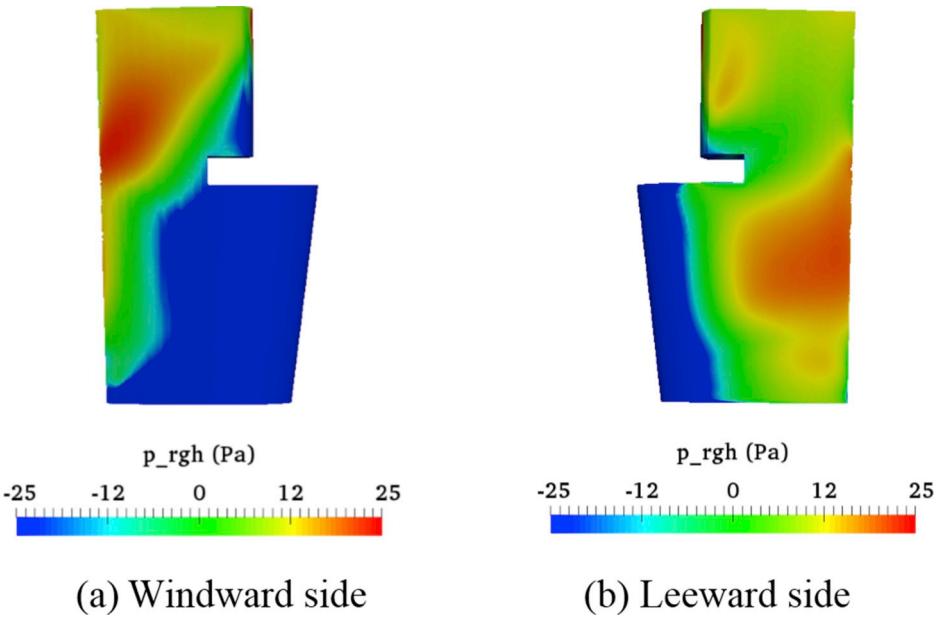

Fig. 13. Pressure distribution on the rudder for RP starboard rudder case (t′ = 18.35) (a) Windward side (b) Leeward side.

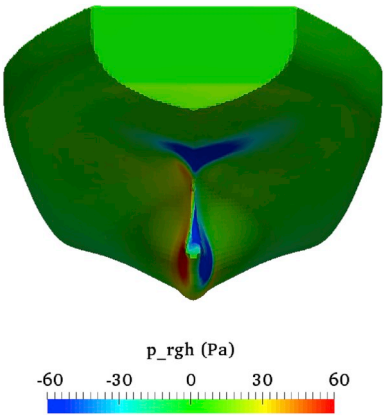

Fig. 14. Pressure distribution on the aft of the ship for RP starboard rudder case (t′ = 18.35).

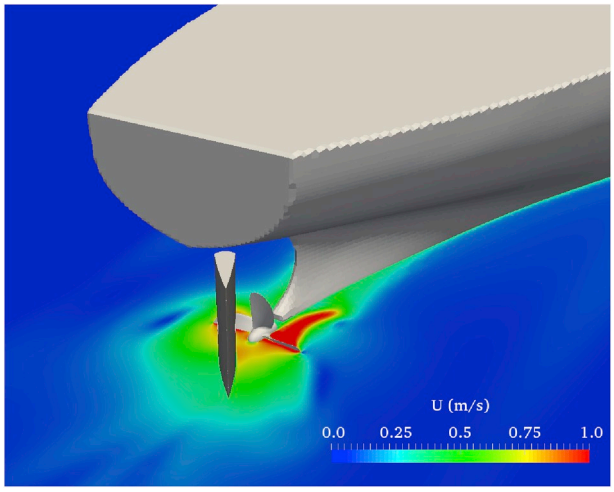

Fig. 15. Wake flow around the propeller and rudder for RP starboard rudder case (t′ = 18.35).

distribution between the opposite sides on the aft hull leads to a lateral force, which pushes the tail to the port side and turns the bow to the starboard side.

Fig. 8 shows the wake flow around ship hull and propeller at the same time instant. The horizontal section demonstrates how the reversing propeller works during the stopping maneuver. The fluid near the propeller is propelled to the front, and the corresponding force in the opposite direction on the propeller slows down the ship speed. It can be seen from Fig. 8b that the propeller propels the fluid around it to the upper right and lower left. The upward moving fluid gathers and impacts on the hull, forming a high-pressure zone on the right aft as shown in Fig. 7. This phenomenon is called the reversing effect.

Turning the rudder to the port or starboard side has great effect on the stopping maneuver using reversing propeller, which is also called the astern port/starboard stopping. In order to investigate the different behaviors for reversing propeller with turning rudders, the conditions of turning rudder to port/starboard side are also simulated. The numerical calculations start from a speed of 0.4905 m/s in model scale. Then the full astern propeller is executed and in the meantime the rudder turns 35° in two different directions with the maximum rudder rate.

Fig. 9 shows the comparison of trajectory and longitudinal velocity between three types of stopping maneuver: reversing the propeller with no rudder and reversing the propeller when turning the rudder to the port or starboard side. So far, there is no experimental data at the same condition to validate the CFD results. Only comparisons between numerical results are presented here. From the simulation results we can see that full astern port will turn the ship to an opposite direction compared with the original no rudder case. The track reach or the stopping distance is around 3.7L and the lateral distance is about 0.47L for the astern port case. Both the track reach and the lateral distance are reduced, with a decrease of 12% and 32%, respectively. As for the astern starboard case, the stopping distance is approximately 4.78L, which is obviously larger than the other two cases. The turning direction for the ship is the same as the no rudder case, while the lateral distance is reduced significantly with a value of 0.22L. Fig. 9b shows the stopping time of the three stopping conditions. The astern port case meets the shortest time to stop the ship, while the astern starboard case experiences the longest time. It can be concluded that the astern port case can stop the ship quickly, while the astern starboard can decrease the lateral distance but with a longer time to stop the ship.

In order to find out the reasons why stopping parameters have the

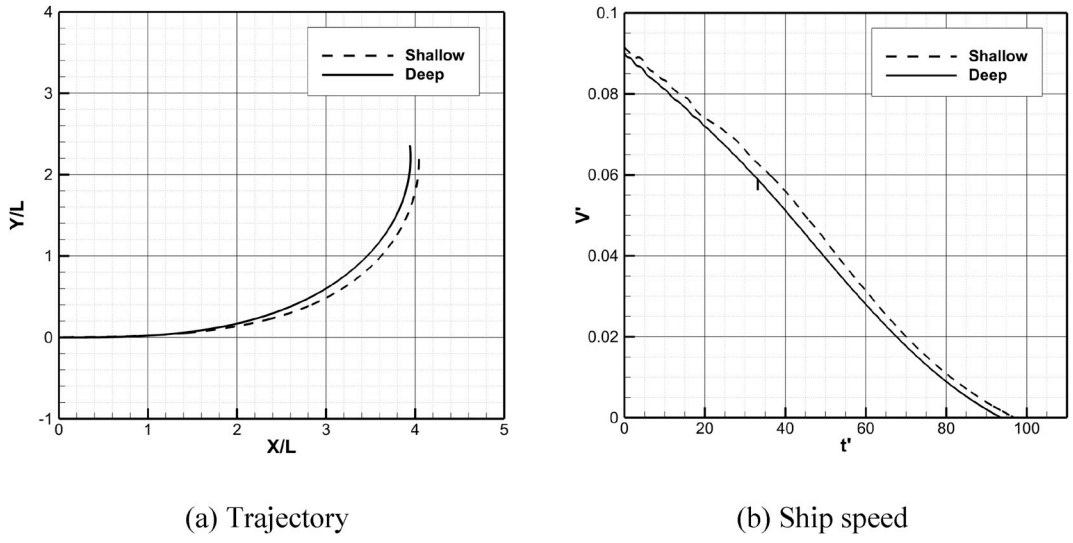

Fig. 16. Trajectory of no engine case under different water depth (a) Trajectory (b) Ship speed.

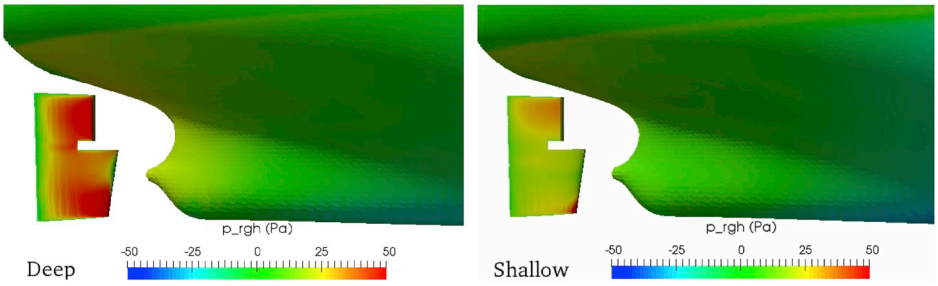

Fig. 17. Pressure distribution on the aft of ship hull and rudder in different water depth.

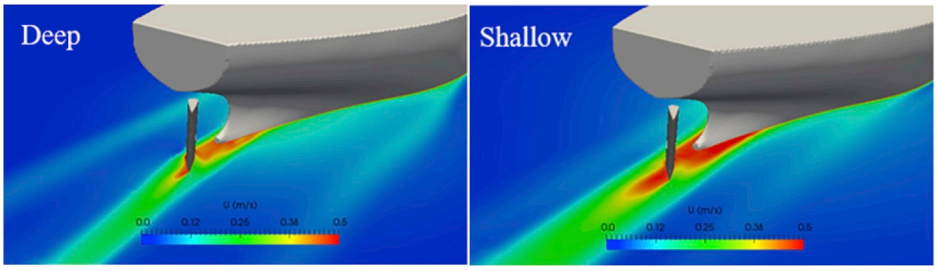

Fig. 18. Wake flow around ship hull and rudder in the inertia stop case.

above changes, the pressure distribution on the stern and wake flow around the ship hull during stopping maneuver are presented and analyzed as follows. The distribution of dynamic pressure in the aft of ship hull for the astern port case is shown in Fig. 10. It can be seen that the reversing effect still exists with a high-pressure zone on the starboard side on the ship hull, while the pressure distribution on the port side is quite complicated. Comparing with the case of no rudder, the amplitude of the high-pressure is smaller. For the port side, the area of low-pressure zone is larger, and as a result, the total transverse force acting on the aft of ship hull pushes the ship stern to port, preventing the ship from turning to port side.

Although the reversing effect exists for the astern port case, the ship still turns to the port side shown in Fig. 9a. Therefore, the rudder effect is stronger than the reversing effect and the rudder force takes the main part in the turning moment. Fig. 11 demonstrates the comparisons of yaw moments between port side rudder and starboard side rudder. The left figure shows the total yaw moment for the ship and the right figure depicts the yaw moment generated by the rudder. It is obvious that the port side rudder can give an overall positive rudder yaw moment for the ship, which explains why the port side rudder can lead to an opposite direction of lateral deviation.

In addition, Fig. 12 shows that the rudder blocks the fluid from being pushing forward. The propelled water on the starboard side has lower speed compared with previous no rudder case, which means that the impact force is smaller, causing lower pressure. The force acting on the rudder makes the ship turn port side, while the side effect caused by reversing propeller has an opposite effect. The comprehensive interaction turns the ship finally to the port side, and the lateral distance is decreased compared with no rudder case.

When conducted astern starboard, the lateral distance is unexpectedly reduced. This can be explained by Fig. 11, where the time histories of yaw moment are compared with the port side rudder case. It can be

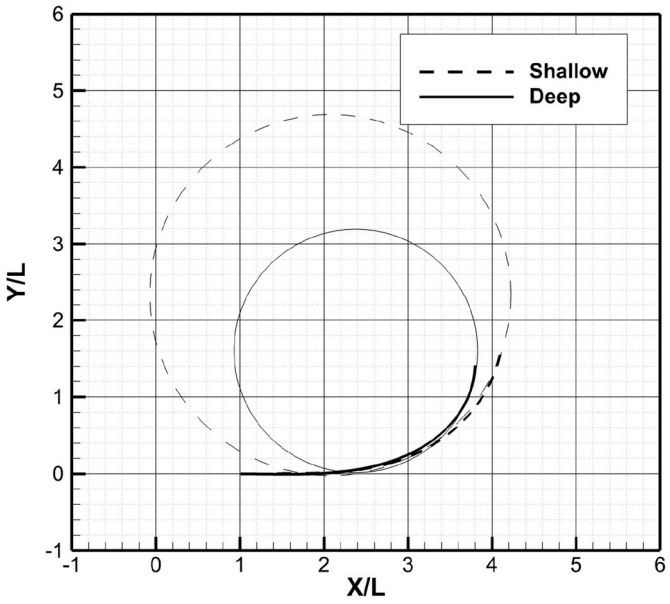

Fig. 19. Trajectory of turning circle maneuver under different water depth.

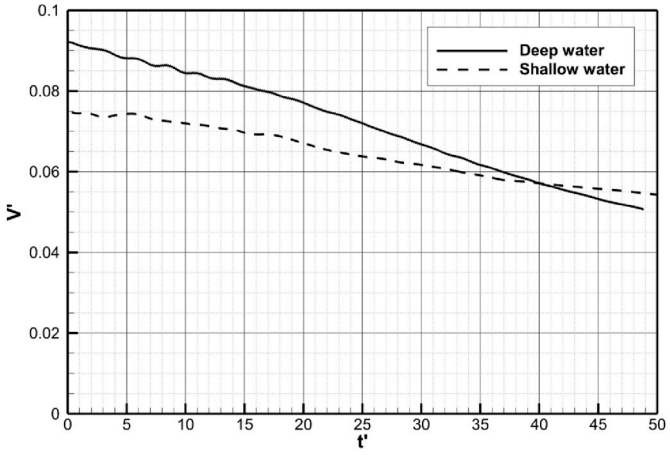

Fig. 20. Ship speed of turning circle maneuver under different water depth.

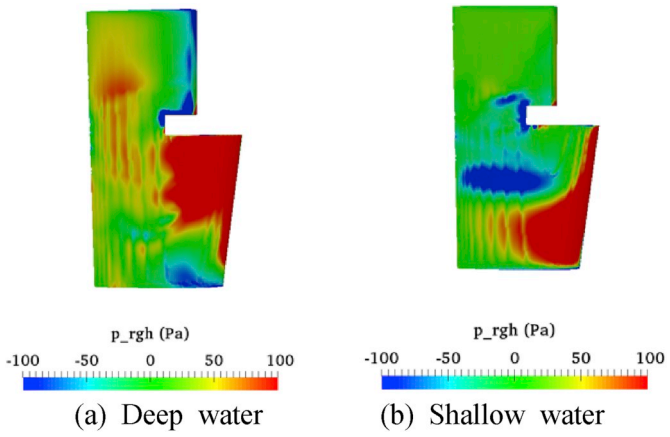

Fig. 21. Pressure distribution on the windward side of rudder under different water depth (a) Deep water (b) Shallow water.

found that the time history of rudder yaw moment is fluctuating around zero, which means that the rudder deflection to starboard side associated with reversing propeller cannot provide effective turning moment to help the ship turn to port or starboard side. This is one of the reasons that the lateral deviation is smaller in the astern starboard case.

In order to explain the rudder effect in the astern starboard case, the distribution of dynamic pressure on rudder is presented in Fig. 13. It can be seen that the pressure distribution is quite complicated for both the windward and leeward side rudder. Reversing propeller accelerates the inflow of the rudder in the forehead of rudder and lead to the high fluid velocity, which results in the lower pressure in the forehead. But high pressure occurs in the after of the rudder due to the downstream wake flow of the ship hull and propeller. The interlacing distribution of positive and negative pressure on the rudder decreases the rudder effect and thus the rudder cannot provide effective turning force.

Fig. 14 shows the dynamic pressure distribution on the aft of ship hull with the astern starboard case. It is obvious that the reversing effect caused by reversing propeller nearly disappears. There is no pressure increasing phenomenon on the starboard side of ship hull. This is another reason that the astern starboard case meets the smallest lateral distance.

Fig. 15 shows the wake flow around propeller and rudder in astern starboard case. It can be noticed that flow velocity around the rudder is very high because of the reversing propeller. The rudder cannot obviously change the velocity of water passing by it. Relatively, the reaction force on the rudder is too small to provide enough pressure to change the course of the ship. Because of the existence of rudder, the direction of propelled water on the right side of the propeller has been changed. There will be little water directly impacting on the ship tail, making reversing effect nearly disappears.

It is concluded that the astern starboard case diminishes the reversing effect. And the reversing propeller makes the rudder effect very bad. Therefore, the longitudinal distance increases, and in the meantime the lateral distance is significantly reduced compared to the no rudder case.

4.3. Inertia stop

Apart from the astern stopping maneuver, an alternative way to avoid the collision with obstacle in the open sea is to stop the engine. In this part, the simulations are performed with no propeller to evaluate the inertia stop performance with the consideration of static propeller during the simulation has little influence on the result. Similarly, three degrees of freedom on the horizontal plane are released with a same initial advancing speed of 0.4905 m/s in model scale. Two cases for the inertia stop condition are carried out the investigate the rudder effect on the performance of stopping maneuver. The rudder executes to 35° in model scale for both port and starboard side. In addition, two different water depth are used in this part to study the shallow water effect on the inertia stop case. In deep water case, the water depth is 5L, while in shallow water case, the water depth is 1.8D, where L stands for the length of ship, D means the draft of the ship. The main difference for the shallow water and deep water case is the boundary condition at bottom, which has been illustrated in section 3.2.

Fig. 16 shows the comparison of trajectory and the time histories of ship longitudinal speed for the inertia stop case using full rudder in different water depth. From the figure we can see that the ship changes its course due to the rudder deflection. Meanwhile the ship speed in longitudinal direction is gradually decreased to zero. In shallow water, the stopping distance is a bit larger than that in deep water, while the lateral distance is smaller. Fig. 16b also shows that the longitudinal speed of ship in shallow water decreases slower than that in deep water. It can be concluded that the shallow water has a bad effect on the maneuverability of ship using the turning rudder.

Flow visualizations, such as pressure distribution, wake flow, are presented to investigate the shallow water effect on the inertia stop case.

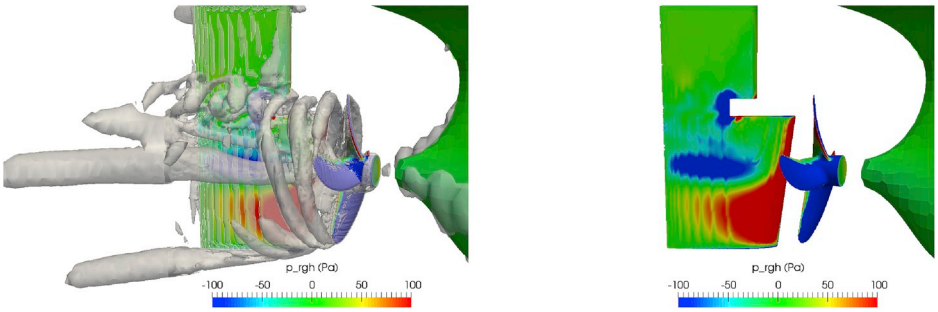

Fig. 22. Vortical structures and pressure distribution around propeller and rudder.

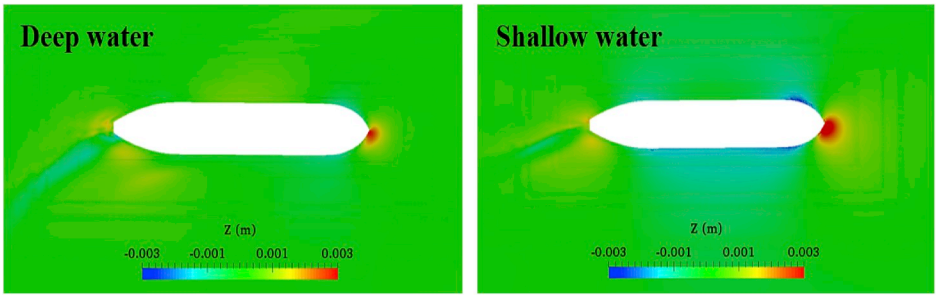

Fig. 23. Comparison of free surface elevation under different water depth ($t' = 24$).

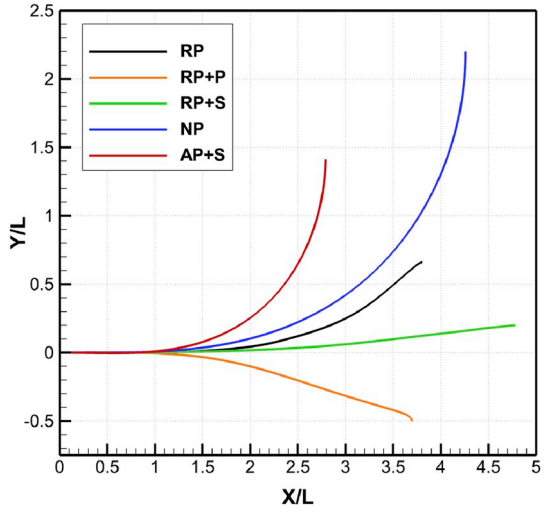

Fig. 24. Comparisons of trajectories of different maneuvers.

The distribution of dynamic pressure on the aft of ship hull and rudder at time instant $t' = 20$ is shown in Fig. 17. It can be seen that the pressure distribution on rudder shows significant difference, where the pressure on rudder is larger in deep water compared with shallow water case. It indicates that the rudder effect is better in deep water and the ship has a relatively bad maneuverability in shallow water. This also corresponds to the turning trajectory shown in Fig. 16a.

Fig. 18 presents the wake flow around ship hull and rudder in both deep water and shallow water case at $t' = 20$. It can be seen that flow velocity after the ship in shallow water is much larger than that in deep water. In shallow water, the relative velocity between fluid and rudder is lower, which means there will be less water impacting on the rudder, resulting in lower pressure. So, the rudder force is decreased in shallow water, making it more difficult to change the course of ship.

4.4. Turning circle

As we all know, turning circle test is the main approach to estimate the ship turning ability. Although the turning circle maneuver with the actual rotating propeller is not a stopping maneuver, it is discussed here due to the fact that it is also used to avoid the collision in the open sea. For ease of comparison with different ways of stopping maneuvers mentioned above, the numerical calculation for the turning circle maneuver also starts from the steady state of self-propulsion. The propeller rate of revolution is set to a constant value of 10.52 r/s, which is obtained from the self-propulsion simulation to reach equivalent between the propeller thrust and the total resistance with corresponding speed of 0.4905 m/s (10kn in full scale). Then turning circle maneuver is achieved by the turning a starboard rudder with 35°. Two different water depth same as section 4.3 are also considered in this part to study water depth effect on the turning behavior. Fig. 19 shows the comparison of turning circle trajectories in different water depth. Since the free running simulation using CFD is very time consuming and the CFD computations only calculate the initial turning stage. The grey lines are extrapolated by the computed results. For the deep water case, the diameter of turning circle in deep water is approximately 2.9*L*, while the turning diameter in shallow water is about 4.3*L*. Here L denotes the ship length. The water depth has a significant effect on the turning circle maneuver, and the shallow water effect is more obvious than the inertia stop condition discussed in sect 4.3. Turning ability in shallow water becomes worse.

Fig. 20 presents the ship speed under different water depth. It can be seen that ship speed in shallow water is significantly lower than that in deep water. Meanwhile, the ship speed in deep water decreases faster, which means the course of ship changes quicker. The turning ability is much better in deep water.

Fig. 21 shows the pressure distribution on the windward side of rudder under different water depth at $t' = 24$. It is obvious that the water depth has great effect on the pressure distribution. The area of high pressure zone in deep water is significantly larger than that in shallow water. Therefore, the rudder effect in deep water is better, which means larger rudder force and larger turning moment.

Apart from the difference of high pressure zone, it can also be found

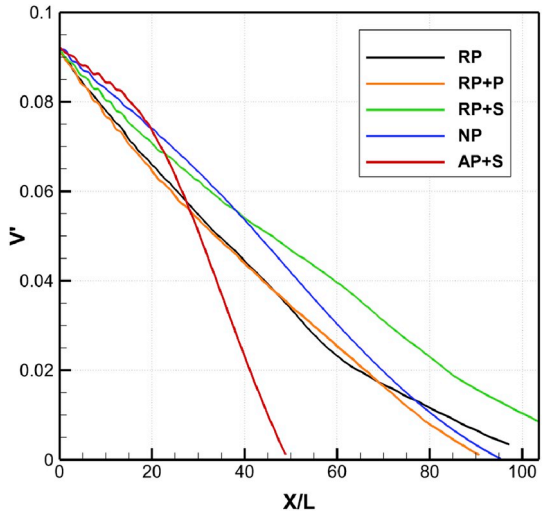

Fig. 25. Comparison of longitudinal speed of different maneuvers.

Table 2
Comparison of main parameters in different maneuvers.

Cases	Track reach X/L	Lateral distance Y/L	Stopping time $t/\sqrt{L/g}$
RP	3.90	0.67	105
RP + P	3.71	−0.50	93
RP + S	4.78	0.21	126
NP	4.27	2.25	96
AP + S	2.79	1.41	50

that there are wavy wiggles of pressure on the rudder surface. In order to explain this phenomenon, the vortical structures around propellers and rudders are presented in Fig. 22. It is obvious that the pressure distribution is strongly affected by the vortices separated from the propeller and rudder. The vortices on the rudder surface are discontinuous and this can explain the pressure wavy wiggles on rudder. This phenomenon happens during the turning motion with large rudder deflection. Similar results can also be found in other CFD investigations regarding turning maneuvers (Jin et al., 2019).

Fig. 23 shows the free surface elevation for the turning circle maneuvers during the steady turn in both deep and shallow water. It is obvious that the wave height of the bow wave in shallow water is higher than that of the deep water case. Generally, the wave-making will be more obvious with the increase of ship speed. However, in this case, the shallow water experiences a lower ship speed, while the bow wave is more severe. It is mainly due to the shallow water effect, where the flow can hardly pass through the ship hull. Therefore, the bow wave is higher and as a result, the wave-making resistance is larger in shallow water case. This explains why the ship speed is smaller at the beginning in shallow water as shown in Fig. 20.

4.5. Comparison of stopping parameters

Fig. 24 and Fig. 25 show the comparison of trajectories and longitudinal ship speeds between different maneuvers in deep water simulated in this paper. In the figures, RP stands for the reversing propeller case, RP + P means reversing propeller with port rudder, RP + S means reversing propeller with starboard rudder, NE means no propeller case (inertia stop case with starboard rudder), AP + S means turning circle with actual rotating propeller and starboard rudder.

It can be seen from Fig. 24 that the RP case with port rudder meets the minimum stopping distance if the KVLCC1 ship model needs to be completely stopped. And the RP case with starboard rudder experiences the minimum lateral deviation. If the ship has no need to be stopped completely, such as the ship advancing in open sea to avoid collision, the turning circle maneuver can be the best choice since it has the minimum track reach.

Fig. 25 shows the longitudinal speed of ship model under different maneuvers. It can be easily seen that the turning circle maneuver with actual propeller and full starboard rudder (AP + S) costs the shortest time to stop the ship, while the RP case with starboard rudder experiences the longest time to stop. Other stopping maneuvers have the similar stopping time. To quantitively analyze the predicted data, Table 2 presents the comparison of the main parameters for the different kinds of ship maneuvers. It can be concluded that the turning circle maneuver is the most preferable way to avoid the collision in open sea since it has the shortest time and minimum advance. If the ship needs to stop in port or waterways, then the reversing propeller (RP) is better with the fact that it meets the relatively shorter later deviation. Among the RP cases, the port rudder can decrease the track reach, while the starboard case will reduce the lateral distance.

5. Conclusions

This paper presents the CFD simulations of KVLCC1 ship model with different maneuvers, i.e. reversing propeller with/without turning rudder, no propeller case (inertia stop case) and the original turning circle maneuver. Shallow water conditions are also simulated to investigate the water depth effects on the ship maneuvers. Numerical computations are carried out using in-house CFD solver naoe-FOAM-SJTU based on overset grid technique. The numerical results of self-propulsion and order astern case with no rudder agree well with the experimental data, showing that the numerical method adopted in this paper is reliable in predicting stopping ability of ship in model scale.

Reversing the propeller can quickly reduce the longitudinal speed of ship. The propelled water affects the distribution of wake flow and the pressure on the aft of ship hull, which further result in the course changing of ship, also known as the reversing effect. In addition, the reversing propeller case with port rudder reduces the stopping distance, while the starboard rudder increases the stopping distance and the lateral deviation is smaller. The reason is that the existence of rudder changes the wake flow around rudder and pressure distribution on ship hull, which diminishes the reversing effect.

Inertia stop case and the traditional turning circle maneuver can be used when the obstacle is far away in open area. It is found that rudder effect is relatively bad in shallow water and the stopping ability of ships in shallow water is worse.

It is concluded that the turning circle maneuver is the most preferable way to avoid the collision in open sea. However, if the ship needs to stop in port or waterways, then the reversing propeller (RP) is better with the fact that it meets the relatively shorter lateral deviation. Among the RP cases, the port rudder can decrease the track reach, while the starboard case will reduce the lateral distance.

In the future, more degrees of freedom can be considered to improve the accuracy of the present CFD simulation. In addition, larger scale ship model should also be simulated to evaluate the scale effects on the stopping maneuver.

Author statement

Jianhua Wang: Conceptualization, Methodology, Software, Writing-Original draft preparation, Data curation, Visualization, Investigation, Validation. Decheng Wan: Supervision, Investigation, Validation, Writing- Reviewing and Editing.

Declaration of competing interestCOI

Our research interest is mainly on Computational Marine Hydrodynamics, Ship Flows, Sea-keeping, Maneuverability, Simulation Based

Design for Offshore and Polar Structures, Renewable Energy in Deep Sea, numerical marine basin, nonlinear wave theory, wave loads on structures, numerical analysis of riser vortex-induced vibration (VIV) and platform vortex-induced motion (VIM), fluid-structure interaction, offshore wind turbine and other offshore renewable resources, as well as high performance computation on complex ship and ocean engineering flows, etc.

Acknowledgments

This work is supported by the National Natural Science Foundation of China (51809169, 51879159, 51490675, 11432009, 51579145), Chang Jiang Scholars Program (T2014099), Shanghai Excellent Academic Leaders Program (17XD1402300), Innovative Special Project of Numerical Tank of Ministry of Industry and Information Technology of China (2016-23/09), National Key Research and Development Program of China (2019YFB1704204) to which the authors are most grateful.

References

Chislett, M.S., Smitt, L.W., 1972. A brief description of the Hya large amplitude Pmm system. J. Mech. Eng. Sci. 14, 80–84. https://doi.org/10.1243/JMES_JOUR_1972_014_067_02.

Muscari, R., Dubbioso, G., Ortolani, F., Di Mascio, A., 2017. Analysis of propeller bearing loads by CFD. Part II: transient maneuvers. Ocean. Eng. 146, 217–233. https://doi.org/10.1016/j.oceaneng.2017.09.050.

Shen, Z., Wan, D.C., 2016. An irregular wave generating approach based on naoe-FOAM-SJTU solver. China Ocean Eng. 30, 177–192.

Shen, Z., Ye, H., Wan, D.C., 2014. URANS simulations of ship motion responses in long-crest irregular waves. J. Hydrodyn. Ser. B 26, 436–446. https://doi.org/10.1016/S1001-6058(14)60050-0.

Wang, J., Zhao, W., Wan, D.C., 2019. Simulations of self-propelled fully appended ship model at different speeds. Int. J. Comput. Methods 16, 1840015, 1–22.

Wang, J., Zou, L., Wan, D.C., 2017. CFD simulations of free running ship under course keeping control. Ocean. Eng. 141, 450–464. https://doi.org/10.1016/j.oceaneng.2017.06.052.

Abkowitz, M.A., 1980. Measurement of hydrodynamic characteristics from ship maneuvering trials by system identification. Trans. - Soc. Nav. Archit. Mar. Eng. 88, 283–318.

Berberović, E., van Hinsberg, N., Jakirlić, S., Roisman, I., Tropea, C., 2009. Drop impact onto a liquid layer of finite thickness: dynamics of the cavity evolution. Phys. Rev. E 79, 36306. https://doi.org/10.1103/PhysRevE.79.036306.

Carrica, P.M., Ismail, F., Hyman, M., Bhushan, S., Stern, F., 2012. Turn and zigzag maneuvers of a surface combatant using a URANS approach with dynamic overset grids. J. Mar. Sci. Technol. 18, 166–181. https://doi.org/10.1007/s00773-012-0196-8.

Carrica, P.M., Mofidi, A., Eloot, K., Delefortrie, G., 2016. Direct simulation and experimental study of zigzag maneuver of KCS in shallow water. Ocean. Eng. 112, 117–133. https://doi.org/10.1016/j.oceaneng.2015.12.008.

Crane Jr., C.L., 1967. Methods to Improve Ship Stopping Performance (No. SIT-DL-69-1208).

Dong, G., Lu, H., Wang, X., 1996. A mathematical model of ship motion and simulative study in crash stopping. J. Shanghai Jiao Tong Univ. (Sci.) 30, 42–48.

Dubbioso, G., Muscari, R., Ortolani, F., Di Mascio, A., 2017. Analysis of propeller bearing loads by CFD. Part I: straight ahead and steady turning maneuvers. Ocean. Eng. 130, 241–259. https://doi.org/10.1016/j.oceaneng.2016.12.004.

Hooft, J.P., 1970. The steering of a ship during the stopping manoeuvre. Int. Shipbuild. Prog. 17, 191–203.

Issa, R.I., 1986. Solution of the implicitly discretised fluid flow equations by operator-splitting. J. Comput. Phys. 62, 40–65.

Jin, Y., Duffy, J., Chai, S., Magee, A.R., 2019. DTMB 5415M dynamic manoeuvres with URANS computation using body-force and discretised propeller models. Ocean. Eng. 182, 305–317.

Lu, D., 2007. Simulation on ship stopping motion by reverse propulsion. Ship Sci. Technol. 29, 110–116.

Menter, F.R., Kuntz, M., Langtry, R., 2003. Ten years of industrial experience with the SST turbulence model. Turbul. Heat Mass Transf. 4, 625–632.

Mofidi, A., Carrica, P.M., 2014. Simulations of zigzag maneuvers for a container ship with direct moving rudder and propeller. Comput. Fluids 96, 191–203. https://doi.org/10.1016/j.compfluid.2014.03.017.

Shen, Z., Wan, D.C., 2013. RANS computations of added resistance and motions of a ship in head waves. Int. J. Offshore Polar Eng. 23, 264–271.

Shen, Z., Wan, D.C., Carrica, P.M., 2015. Dynamic overset grids in OpenFOAM with application to KCS self-propulsion and maneuvering. Ocean. Eng. 108, 287–306. https://doi.org/10.1016/j.oceaneng.2015.07.035.

Tsukada, Y., Ueno, M., Tanizawa, K., Kitagawa, Y., Miyazaki, H., Suzuki, R., 2015. New free-running model ship tests using auxiliary thruster. Pap. Natl. Marit. Res. Inst. 15, 255–279.

Ueno, M., Suzuki, R., Tsukada, Y., 2017. Estimation of stopping ability of full-scale ship using free-running model. Ocean. Eng. 130, 260–273. https://doi.org/10.1016/j.oceaneng.2016.12.001.

Wang, J., Wan, D.C., 2018. CFD investigations of ship maneuvering in waves using naoe-FOAM-SJTU solver. J. Mar. Sci. Appl. 17, 443–458. https://doi.org/10.1007/s11804-018-0042-4.

Wang, J., Zou, L., Wan, D.C., 2018. Numerical simulations of zigzag maneuver of free running ship in waves by RANS-Overset grid method. Ocean. Eng. 162, 55–79. https://doi.org/10.1016/j.oceaneng.2018.05.021.

Wang, J., Zhao, W., Wan, D.C., 2019. Development of naoe-FOAM-SJTU solver based on OpenFOAM for marine hydrodynamics. J. Hydrodyn. 31 (1), 1–20. https://doi.org/10.1007/s42241-019-0020-6.

Yabuki, H., Yoshimura, Y., Ishiguro, T., Ueno, M., 2006. Turning motion of a ship with single CPP and single rudder during stopping maneuver under windy condition. In: Proceedings of International Conference on Marine Simulation and Ship Manoeuvrability. Terschelling, the Netherlands.

Yasukawa, H., Yoshimura, Y., 2015. Introduction of MMG standard method for ship maneuvering predictions. J. Mar. Sci. Technol. 20, 37–52. https://doi.org/10.1007/s00773-014-0293-y.

Zha, R., Ye, H., Shen, Z., Wan, D.C., 2014. Numerical study of viscous wave-making resistance of ship navigation in still water. J. Mar. Sci. Appl. 13, 158–166. https://doi.org/10.1007/s11804-014-1248-8.

Zha, R., Ye, H., Shen, Z., Wan, D.C., 2015. Numerical computations of resistance of high speed catamaran in calm water. J. Hydrodyn. Ser. B 26, 930–938. https://doi.org/10.1016/S1001-6058(14)60102-5.